Formation of covalent di-tyrosine dimers in recombinant α-synuclein

A van Maarschalkerweerd[1,†], MN Pedersen[1,†], H Peterson[1], M Nilsson[1], TTT Nguyen[2], T Skamris[1], K Rand[2], V Vetri[3], AE Langkilde[1], and B Vestergaard[1,*]

[1]Department of Drug Design and Pharmacology; University of Copenhagen; Copenhagen, Denmark; [2]Department of Pharmacy; University of Copenhagen; Copenhagen, Denmark; [3]Dipartimento di Fisica e Chimica; Universitá di Palermo; Palermo, Italy

[†]These authors equally contributed to this work.

Parkinson's disease is associated with fibril deposition in the diseased brain. Misfolding events of the intrinsically disordered synaptic protein α-synuclein are suggested to lead to the formation of transient oligomeric and cytotoxic species. The etiology of Parkinson's disease is further associated with mitochondrial dysfunction and formation of reactive oxygen species. Oxidative stress causes chemical modification of native α-synuclein, plausibly further influencing misfolding events. Here, we present evidence for the spontaneous formation of covalent di-tyrosine α-synuclein dimers in standard recombinant protein preparations, induced without extrinsic oxidative or nitrative agents. The dimers exhibit no secondary structure but advanced SAXS studies reveal an increased structural definition, resulting in a more hydrophobic micro-environment than the highly disordered monomer. Accordingly, monomers and dimers follow distinct fibrillation pathways.

Introduction

Neurodegenerative diseases such as Parkinson's (PD), Alzheimer's and Huntington's diseases are all associated with inclusions of aggregated proteins in the human brain.[1] PD pathology is characterized by progressive death of primarily dopaminergic neurons in the *substantia nigra pars compacta* in the mid brain[2] which is associated with the presence of Lewy bodies (LB).[3] LB are found in connection with PD and a number of related diseases[3,4] and its major constituent is fibrillated α-synuclein (αSN). αSN is a 140 amino-acid intrinsically disordered protein[5,6] which allegedly is involved in synaptic exocytosis through its role in the formation of SNARE protein complexes.[7-9] For yet unknown reasons, αSN is prone to form amyloid fibrils, and recent results suggest that such aggregates spread intercellularly in a prion-like manner.[10] Although the presence of LB is clearly linked to PD, it is suggested that intermediate pre-fibrillar structural αSN species exert cytotoxicity *in vivo*.[11-13] The propensity of *in vivo* LB formation is influenced by a number of genetic factors such as point mutations in the gene encoding αSN or even multiplication of it.[14,15] Never the less, idiopathic PD is by far the predominant form of PD,[2,16] but the issue of why and how wild-type αSN initiates pathological fibrillation is largely an unsolved mystery despite the immense interest into the subject (for recent reviews, see e.g. Lashuel et al.[4] and Breydo et al.[17]). There is currently no cure for PD and pharmacological treatment is yet only symptomatic.[2] Understanding the triggering factors behind structural alterations of αSN leading to cytotoxic events is hence essential in order to rationalize future drug design strategies.

Numerous studies have shown that αSN is subject to chemical modifications under nitrative and oxidative stress.[18-21] These modifications are typically associated with the four tyrosine-residues Y39, Y125, Y133 and Y136. This is particularly interesting in the light of accumulating evidence that the pathogenesis of PD is linked to oxidative stress, mitochondrial dysfunction, and

formation of reactive oxygen species.[22-27] αSN is an intrinsically disordered protein, which however does not equal an unstructured state.[28] Several studies address the structural distribution of αSN both *in vitro*[29,30] and in cell,[31] revealing structural sensitivity to both the presence of lipids and detergents[30,32] or the presence of metal ions.[33] Likewise, chemical modification will alter the structural preferences of αSN, and thus influence fibrillation propensity.

The findings from the present study suggest that αSN is more prone to chemical modification than previously assumed. We highlight *in vitro* findings showing that αSN is subject to significant chemical modification by di-tyrosine cross-linking even in the absence of extrinsic oxidative and nitrative agents. Rather, we demonstrate the formation of covalent αSN dimers under mild *in vitro* conditions, and we characterize the particular structural features of the novel dimer primarily by combined size exclusion chromatography (SEC) and Small-Angle X-ray Scattering (SAXS) analysis. By means of liquid chromatography coupled to mass spectrometry (LC-MS) we identify a covalent cross-link between two Y39 residues. We argue that this observed chemical modification at least in part is responsible for dimer formation and that such dimerization very likely relates to the loss of native function and possibly also relates to altered propensity for formation of cytotoxic aggregates.

Results

The purification protocol for recombinant αSN employed in this publication is an optimized protocol,[34,35] widely used in the field.[36-38] Recombinant αSN is exported to the periplasm of the expressing bacterial cells and it is hence possible to explore release by osmotic shock, which results in reduced amounts of impurities as compared to full cell lysis.[34] Concomitant purification steps including boiling, ion-exchange chromatography and SEC are commonly used to obtain high yields of pure αSN.[34-38] Of these

steps, SEC is critical to obtain high purity of the crude product, but it is not in itself considered to be a possible cause of any structural artifacts. In **Figure 1A** we present the chromatographic traces (UV$_{280nm}$) of αSN eluting from the SEC-column. Due to the unfolded nature of αSN, the protein elutes in a much larger elution volume than a corresponding folded protein of the same molecular mass.[4,34] Importantly, the injected net amount of protein (resulting in protein batches αSN type0–3) has a clear impact on the shape of the elution peak containing αSN, indicated by the arrow in **Figure 1A**. We immediately note that the species that is formed during the last purification step, is not formed during any of the prior purification steps (such as e.g. e.g., the boiling step) since type0 is seemingly devoid of the species. The eluting fractions were pooled, dialyzed, lyophilized and re-dissolved (in accordance with the standard purification protocol) prior to all subsequent analyses.

To assess the nature of the altered αSN species, we used ANS. ANS is a fluorescent dye used to probe protein conformational reorganizations associated with changes in the solvent exposure of hydrophobic regions, to detect and characterize non-polar surface patches of proteins, non-native partially folded conformations of globular proteins and to detect and to monitor the formation of molten globule-like species.[39,40] An increase in the fluorescence intensity and a blue-shift on the emission spectrum are usually observed upon binding of ANS to either exposed hydrophobic regions or hydrophobic clusters.[39]

Figure 1B shows the gradual increase of ANS fluorescent emission after addition to the protein batches. The ANS fluorescence is clearly increasing, meaning that different samples have different affinity with the dye and that the ANS microenvironment is characterized by different properties which result in higher fluorescence signal, in the order type3>type2>type1.[40]

Circular dichroism (CD) did not reveal any difference between type 0–3 samples, with all spectra being typical of random coil (**Fig. 2**). The increase in ANS affinity was hence not associated with induction of secondary structural elements. Intrinsic fluorescence, however, revealed a significant difference. The 3D fluorescence spectrum of a type3 batch is shown in **Figure 2B**. The type3 profile has an in part comparable signal to the other samples in the same conditions. The tyrosine signal is clearly observable as the high intensity peak in the emission range 290–350 when excitation wavelength is below 300 nm. Importantly, a significant emission band centered at about 400 nm is observed at excitation wavelengths above 280 nm. This signal corresponds with previous reports of chemically induced *o-o'*-di-tyrosine formation in αSN[19-21] The same measurements on type0, type1 and type2 αSN samples reveal the presence of the same peak with type0 exhibiting the weakest signal (not shown). The increase in ANS fluorescence is thus
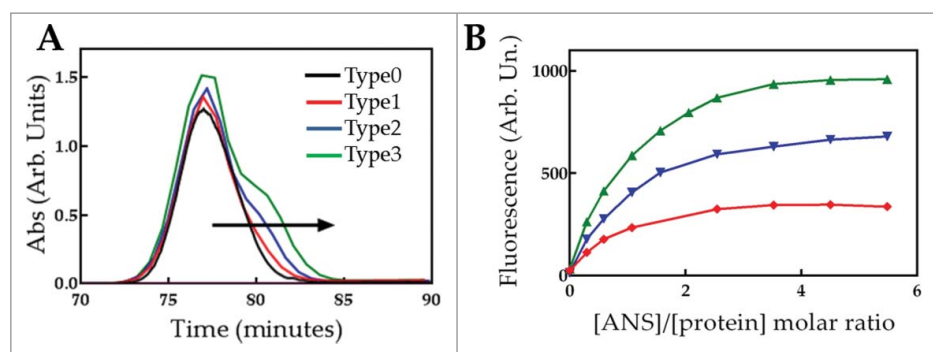
Figure 1. Initial characterization of the αSN batches after variation in the purification procedure. (**A**) The UV$_{280nm}$ trace of the final SEC step of the purification of recombinant αSN. 2 mL eluent from the ion-exchange chromatography were injected on the HiLoad Superdex 200 SEC column in concentrations of 3.5, 5.5 8.0 and 10 mg/ml to obtain αSN type0 (black curve), type1 (red curve), type2 (blue curve) and type3 (green curve), respectively. The arrow indicates the increasing size of the late eluting shoulder (**B**) ANS titration of αSN type1 (red), type2 (blue) and type3 (green) depicting increasing ANS fluorescence intensity.

likely due to the transient formation of hydrophobic pockets, associated with the di-tyrosine formation. Increase in ANS fluorescence from evolving fibrillating samples have previously been coupled to increased toxicity.[40] We therefore tested if type3 samples could disrupt vesicles with higher potency than type0 samples, which, however was not the case (**Fig. S1**).

The *in vivo* fibrillation of αSN and the deposition of amyloid fibrils in LB is a central phenomenon related to the pathogenesis of PD. Here, we investigated if the changes induced during SEC influences the *in vitro* fibrillation process of αSN. In **Figure 3** we present the fibrillation profiles of αSN type0–3, monitored by ThT fluorescence. The fibrillation was performed at identical protein concentrations for all protein batches, and the concentration was chosen above the supercritical concentration.[37] We observe no significant differences in the ThT-monitored fibrillation kinetics between type0, type1 and type2. However, the fibrillation profile of αSN type3 is clearly altered. Type0, type1 and type2 present the classical sigmoidal profile, which reaches a stable plateau value indicating that an equilibrium state is reached in the sample. The aggregation profile of type3 samples shows significant differences: after a first

sigmoidal growth phase within the first 10 hours, a second growth phase is observable which does not reach a plateau value within the observation time reported here.

To investigate if these two kinetic phases in the fibrillation assay resulted in different fibril structures, the fingerprint of the fibril atomic structure was investigated with X-ray fiber diffraction, which however did not reveal any differences between the most prominent repeating distances in the internal fibril structures (**Figs. S2 and S3**).

To assess the possible structural differences between the protein batches, we subsequently performed SAXS analysis. Primary SAXS analysis was performed on freshly dissolved αSN type0–3 to investigate if the overall dimensions differed in the batches. For each type we evaluated 3 concentrations, and revealed no concentration effects within each type0–3. However, clearly, the overall appearances of the 1-dimensional scattering profiles (**Fig. 4A**) were differing between the protein batches. We thus evaluated the
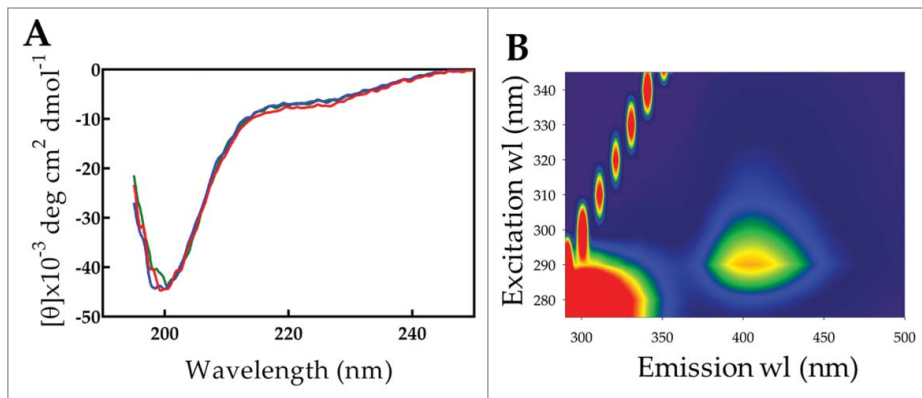
overall radius of gyration (R_g) and average molecular mass (proportional to the extrapolated forward scattering, I(0)) (**Fig. 4B**). For both parameters a stepwise increase is observed in the order type3>type2>type1>type0. This corresponds to a gradual increase in the average oligomeric state in αSN type0–3, which hence suggests that the previously observed formation of a di-tyrosine bond is intermolecular and not intramolecular. The relatively modest increase in average molecular weight suggests that the oligomeric form is a dimer. We observe no concentration dependent effects on the average molecular weight (data not shown), and can

Figure 2. Preliminary biophysical characterization of type0–3 preparations. (**A**) Far-UV CD measurements on readily dissolved αSN type1 (red curve), type2 (blue curve) and type3 (green). (**B**) 3D scan of Intrinsic fluorescence of type3 αSN.
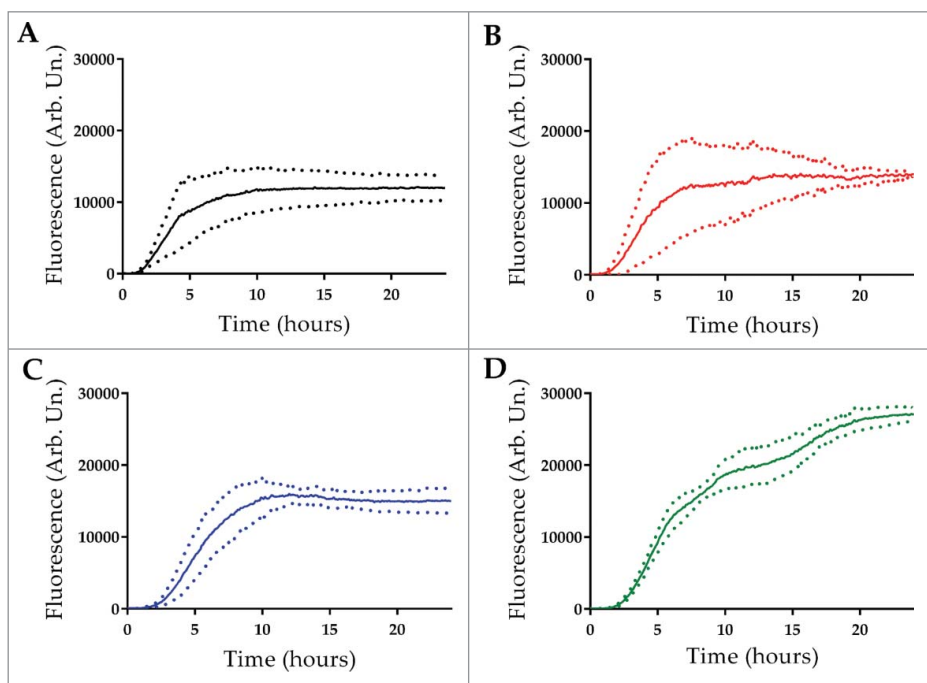

Figure 3. Fibrillation kinetics of 12 mg/ml αSN were monitored using 20 μm ThT as *in situ* probe. Measurements were performed in triplicate of αSN type0 (black curve), type1 (red curve), type2 (blue curve) and type3 (green curve). The averaged curves are shown as full lines and the dotted lines indicate the standard deviation.
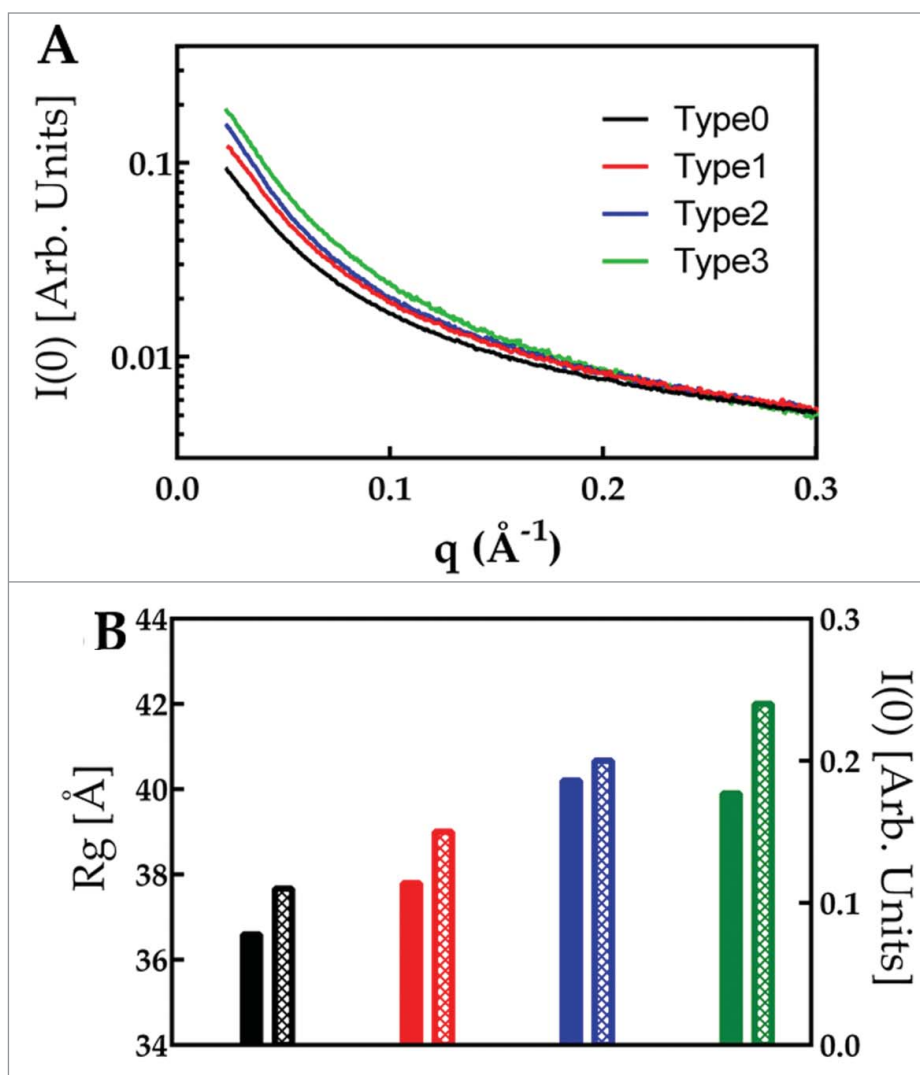
Figure 4. Basic parameters derived from SAXS show increasing global average dimension of αSN type0–3. The 1D scattering curves (**A**) were analyzed in order to obtain the R_g and I(0) (**B**). The R_g (filled bars, left axis) and I(0) (empty bars, right axis) of αSN are shown for type0 (black), type1 (red), type2 (blue) and type3 (green).

conclude that the dimers are covalently formed. This can be concluded since non-covalent oligomerisation is strictly concentration dependent.

The 3D structure of an intrinsically disordered protein, such as αSN, is not adequately described by a static structural model. To obtain a more detailed structural interpretation, we employed the program Ensemble Optimization Method (EOM), by which the experimental data are fitted to ensembles of structures from a large pool of possible conformations (**Fig. S4**). One pool describing αSN as a fully flexible monomer was generated as well as 3 different pools of possible αSN dimer constructions (see materials and methods for details), and the EOM analysis was performed, allowing sampling from both monomer and dimer pools. For αSN type1–3, a proportion of dimer structures were selected in the optimization (**Table 1**) and the presence of dimers in the selected ensemble gradually increased with the increasing

presence of a shoulder in the SEC profiles (i.e. type3 reflecting the highest dimer content), while the optimized ensemble, which fits the type0 scattering did not include dimer structures. This is fully in accordance with the observed increase in average molecular weight hence the EOM fitting further corroborates our suggestion, that dimers are formed in type1–3. This result from the ensemble fitting is fully complementary to the basic observation of increased molecular weight and increased radius of gyration. We conclude that the SAXS and EOM analysis of the protein batches strongly support the notion of dimerization

To look for a covalent cross-linking in αSN we performed a peptide mapping analysis by LC-MS/MS for αSN type3 and type0, respectively. Sequence coverage of the protein was 69–73% (type3) and 57–64% (type0) with the missing coverage locating in the C-terminal (103–140).

Among the multitude of tryptic peptides, two were identified containing Y39, herein referred to as peptide "*G*" (residue 33–43) and peptide "*F*" (residue 33–45). To investigate the existence of a Y39-Y39 crosslink, the MS data were analyzed for ion masses corresponding to all theoretical combinations of di-tyrosine crosslinks of these two peptides. Ion masses corresponding to $F + F$ [$(M + 5H)^{5+}$ (*m/z* 472.463), $(M + 4H)^{4+}$ (*m/z* 590.329), $(M + 3H)^{3+}$ (*m/z* 786.771) at R_t = 10 min] and $F + G$ [$(M + 4H)^{4+}$ (*m/z* 533.043), $(M + 3H)^{3+}$ (*m/z* 710.039), $(M + 2H)^{2+}$ (*m/z* 1065.086) at R_t = 11 min were found in the MS spectra of both type3 and type0 samples (mass accuracy of less than 9 ppm).

To further confirm these cross-linked peptides, fragmentation of these peptides by electron transfer dissociation (ETD) was performed. Ions with *m/z* 472 and 590 ($F + F$) as well as *m/z* 533 and 710 ($F + G$) were chosen for fragmentation. **Figure 5** displays an ETD MS/MS mass spectrum of precursor ion *m/z* 533 in the type3 sample. The most abundant fragment ions can be assigned correspondingly to the cross-linked peptide $F + G$. No valuable data were obtained from ETD spectrum of *m/z* 710 as the fragmentation was not efficient for this ion. Furthermore, ETD MS/MS spectra of ions *m/z* 472 and 590 also suggested the existence of $F + F$ peptide (data not shown). The intensity of identified $F + F$ (m/z 590) and $F + G$ (m/z 533) cross-linked peptide ions were higher in type3 than in type0 samples (approx.

Table 1. Types of selected structures from EOM after fitting the scattering of native type0–3 with pools consisting of αSN monomers and 3 different dimer pools, respectively, with contact point in either the C-terminal, from Y39 to Y39 or within the NAC-region. Whereas Type0 is solely described by an ensemble composed of monomers, increasing amounts of dimers are selected in the ensemble describing type1–3

Pools	No. of selected monomer/dimer structures			
	Type0	Type1	Type2	Type3
Monomer / C-terminal dimer	20/0 (X^2=1.131)	17/1 (X^2=1.046)	12/6 (X^2=0.997)	8/6 (X^2=1.111)
Monomer / Y39 dimer	22/0 (X^2=1.148)	18/2 (X^2=1.040)	14/10 (X^2=1.006)	7/15 (X^2=1.106)
Monomer / NAC-region dimer	18/0 (X^2=1.117)	30/6 (X^2=1.032)	16/6 (X^2=0.996)	11/13 (X^2=1.090)

2-fold) relative to other peptides from these 2 samples that showed similar ion intensities (data not shown). Despite the absence of a more rigorous quantitative analysis, these results indicate that the amount of αSN dimers in type3 is greater than in type0. The detection of the Y39-Y39 cross-linked peptide firmly establishes the presence of o-o'-di-tyrosines in the αSN samples investigated. We note with interest, that the covalent bond is formed in close vicinity of point mutations associated with hereditary early-onset PD[14,15,47,48].

In order to investigate the structural nature of the newly identified Y39-Y39 dimer, we employed SEC-SAXS. αSN was up-concentrated before being loaded onto an in-line SEC column.[41] As with the initial purifications (see **Fig. 1A**), we did not have baseline separation. But we have previously shown that we can isolate individual scattering components using the identification of residual data after linear combinations of data from pure species.[37,42] Here we use the same principle for the SEC-SAXS data except that we do not require mass conservation, since protein elutes at varying concentrations over the elution profile (please see materials and methods for details). Two components were necessary to fit the set of experimental data, as evidenced by the large residual scattering profiles from a one-component fitting (**Fig. 6A**).

To select the second component, the peaks in the chromatogram were fitted (see materials and methods) using initial estimates of the second species from data curves highly unlikely to contain fractions of the first component, assuming a Gaussian elution profile for each of the two species (**Fig. 7A**). After applying 2 components in a linear combination throughout the elution profile, the residual scattering was negligible (**Fig. 6B**).

The scattering profiles for the 2 components are shown in **Figure 7B**, clearly proving a larger R_g and a larger apparent molecular mass compared to the first component (**Fig. S5**), hence in accordance with the previous indications from bulk SAXS measurements. Based on the extrapolated forward scattering I(0), we confirm that the first component is the monomer and estimate that the second is the dimer, in agreement with the MS data (**Fig. S5**). From the Pair Distance Distribution Function (PDDF) (**Fig. 7C**), it can be seen that the dimers share many similarities with monomers, but that there is a unique dimer feature between roughly 150 Å and 200 Å. Both the monomer and the dimer appear intrinsically disordered in the Kratky plot (data not shown), which means that static representations of their structures are not valid. This is in agreement with results from MS which have shown that dimers formed above pH 4 are unstructured.[43] The extra feature in the PDDF can therefore not be related to distances between 2 static domains, but describes typical distances between the overall positions of the highly flexible individual
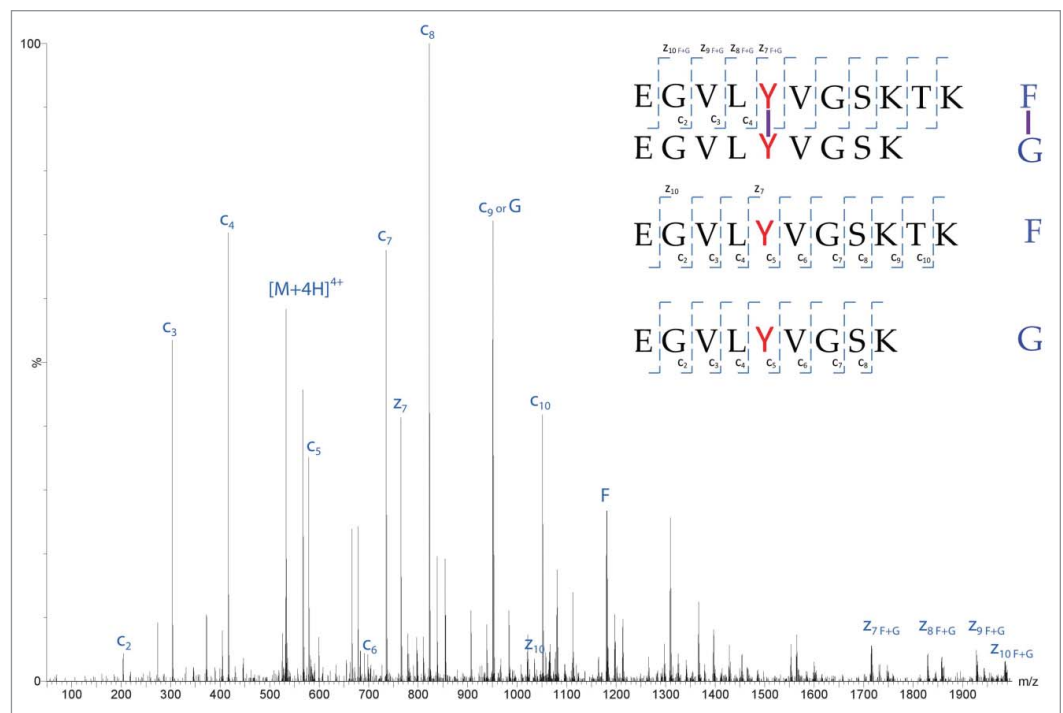

Figure 5. Full ETD fragmentation spectrum of isolated F+G peptide including the Y39-Y39 cross-link. The precursor ion is indicated ([M+4]$^{4+}$).
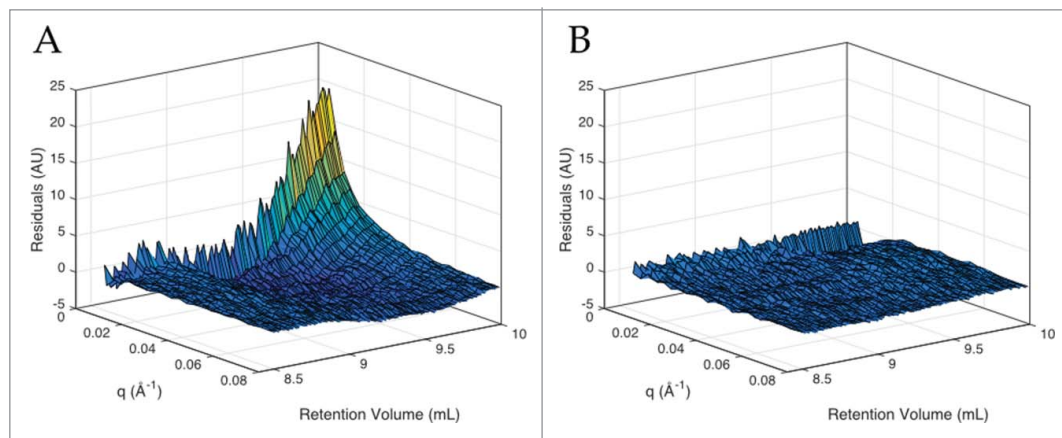
Figure 6. Residuals from the decomposition of the SAXS data from the eluting monomer-dimer peak from the SEC column. The first axis depicts elution volumes, the second axis the q-range and the third axis depicts the scattering intensities. (**A**) The residuals from decomposing the data using one component. (**B**) The residuals from the decomposition using both monomer and dimer data. The color scaling is the same in both plots, ranging from blue to yellow, with brighter colors representing higher scattering intensities.

protein chains in the dimer. To characterize this dimer further, we used EOM to determine ensembles describing the distribution of R_g and maximum distances and thus the nature of the dimer (**Figs. S7 and S8**), this time taking into account the positive identification of Y39-Y39 cross-links, hence sampling only from this specific dimer pool. Likewise, the data corresponding to the monomeric form was analysed analyzed using EOM. The distributions of D_{max} values from the selected ensembles for monomer and dimer data, respectively, are shown in **Figure 7D**. The selected ensemble for the dimer has a main peak centered at approximately 140 Å but also many conformations resulting in maximal distances in the region between 150 Å and 200 Å. The unique dimer feature in the PDDF hence arises from the fraction of dimers exhibiting more elongated structures. With **Figure 7E, F** we further visualize the distinct differences between the monomer and Y39-Y39 covalent dimer forms of αSN. We show how the overall distribution of R_g values is very different for these 2 populations. Each colour color represents one calculated ensemble, which hence has been fitted to the data in the individual runs in EOM, and the size of each dot represents the frequency of the selected conformation within the calculated ensemble. That is, if a colored dot is large, then one particular conformation is very often selected within a given ensemble. The distribution for the monomer is broad and importantly, many different conformations are selected, as visualized by multiple small dots in each ensemble. This means that the monomer pool, which fits to the data, is best described as an ensemble of near-random conformation. Remarkably, this is not the case for the Y39-Y39 dimer, where consistently just a few conformations can represent the structural ensemble. This thus suggests that the dimeric structure is more defined than the monomeric structure, in accordance with the appearance of a defined hydrophobic region, as revealed by ANS binding.

It is of interest to further investigate these frequently occurring individual structures, representing the Y39-Y39

dimer conformations. In the graphical abstract, we have plotted the spatial superimposition of all selected conformations for both the monomer and dimer αSN. An optimized spatial super-position results in a widely distributed cloud of dimeric structures, with individual structures that are even less alike than the large number of widely distributed random monomeric structures. The exception to this is a small, distinguishable structural core in the vicinity of the dimeric bond. We can hence conclude that the induced dimeric structure consists of a hydrophobic core, with the remaining structure in a limited number of preferred conformations, but that these individual conformations are highly diverse. Notably, this type of structural distribution is not to be mistaken for a random distribution of conformation. Rather, such a diverse, yet defined pool is an interesting structural distribution, significant for IDP structure, and complementary to more statically defined 3-dimensional protein structures.

Discussion

Amyloid disease progression is a multifactorial phenomenon, influenced by factors as different as disease-specific point-mutations, mitochondrial dysfunction, and hampered chaperone-mediated folding control.[4] In the case of PD, massive dopaminergic neuronal decay plays a significant role in the disease progression, and the formation of LB, which are rich in αSN fibrillar aggregates, is a hallmark of the disease. Even if the presence of LB does not directly correlate with disease progression,[44-46] overexpression and certain point mutations lead to earlier and more severe development of PD.[47,48] This strongly suggests that αSN somehow plays a central role in the disease pathogenesis and makes the careful study of αSN in its native and aggregated states pivotal for the development of new therapeutic strategies. Here, we reveal the formation of a covalent Y39-Y39 dimer, which influences fibrillation kinetics. It is remarkable that the specific linkage occurs in the vicinity of the positions of early-onset PD point mutations.

Scientific literature is rich in different protocols for the purification of recombinant αSN for *in vitro* studies. The last steps are typically ion-exchange and gel-filtration chromatography, while varying methods are used before these final steps to remove the bulk of protein contamination. Heating is used in some

studies,[36,37] acid denaturation in others,[36] and recombinantly added histags, binding to immobilized copper or nickel, are also used.[49] In terms of removing other contaminant proteins, all above methods are highly efficient. But the purity in terms of oligomeric species is just as important. To our knowledge, neither of the above methods is more prone to induce oligomerisation than the other, and indeed we do not observe that the earlier steps in the purification protocol cause significant formation of oligomeric species. Rather, to our surprise, we observe that up-concentration and subsequent gel-filtration can induce covalent Y39-Y39 dimers.

Furthermore, we provide a structural characterization of the covalent dimer. The altered structure leads to increased ANS binding, which indicates protein conformations with higher affinity to the dye. The detailed analysis of the isolated dimer structural ensemble demonstrated that the dimer remains intrinsically disordered, but

Figure 7. Data from the SEC-SAXS experiments. (**A**) The UV$_{280nm}$ trace from the concentrated sample injected on the gel-filtration column. The black and orange curves are initial Gaussian estimates of the elution of first and second components, respectively. (**B**) The isolated data curves from the first part of the peak corresponding to an αSN monomer (black), and the data curves from the last eluting fractions corresponding to an αSN dimer (orange). (**C**) The average pair distance distribution functions (PDDF) for the monomer (black) and dimer (orange). (**D**) Results from the EOM analysis: The distributions of maximum dimensions in the selected ensembles for the monomer (black) and dimer (orange) respectively. Error bars are the standard deviations from 12 runs. Please cf. supplementary information for a comparison between the initial random pool and the selected ensemble (**Figs. S6 and S7**). (**E–F**) Results from the EOM analysis of the monomer (**E**) and dimer (**F**) data: Maximum distance plotted as a function of the radius of gyration. The colors represent the 12 different runs and the size of the sphere represent the frequency by which the given D$_{max}$/R$_g$ values were selected. Note that far fewer conformations are selected for the dimers, than ditto of the monomer, and the dimensions are on average larger.

that the ensemble of conformations is smaller than the monomer, which must be due to the restrictions imposed by the covalent crosslink (**Fig. 7E, F**). It is hence essential to note that the dimerization induces a structurally more defined state of the otherwise intrinsically disordered protein. In spite of the observation of a more defined structure, CD did not reveal the formation of any secondary structural elements in the dimer, yet the structural change might alter intrinsic function, and modify solution behavior, which would explain the biphasic aggregation kinetics.

Formation of αSN *o-o'*-di-tyrosines has been observed before as a consequence of chemical or mechanical/environmental stress.[18-21,50,51] The typical method for preparing di-tyrosines has however involved strongly oxidative agents such as hydrogen peroxide, which is distinct from the current observation of a covalent dimer formed under mild experimental conditions. Likewise, the dimer is not formed under stress (such as e.g. the boiling step earlier in the purification procedure), rather the species is formed in response to concentration and subsequent gel filtration. The presence of di-tyrosines has previously and in the present study been confirmed using intrinsic fluorescence, because *o-o'*-di-tyrosines exhibit an emission peak around 400 nm when excited at approximately 290–300 nm.[52-54] Oxidation of methionines can also occur when using oxidants, and these oxidized species have been shown to hinder fibrillation.[55] The exact chemical nature of such species may not be identified by intrinsic fluorescence and we recommend that investigations of oxidation products include MS. Here, by MS we exclusively detect the existence of Y39 cross-linked dimers, in opposition to unselective tyrosine cross-linking, which has been observed when oxidizing reagents are employed.[18,19] As a note, the MS/MS analytical coverage is reduced in the C-terminal part of αSN, due to the lack of trypsin cleavage sites, hence potential additional C-terminal cross-links might remain undetected.
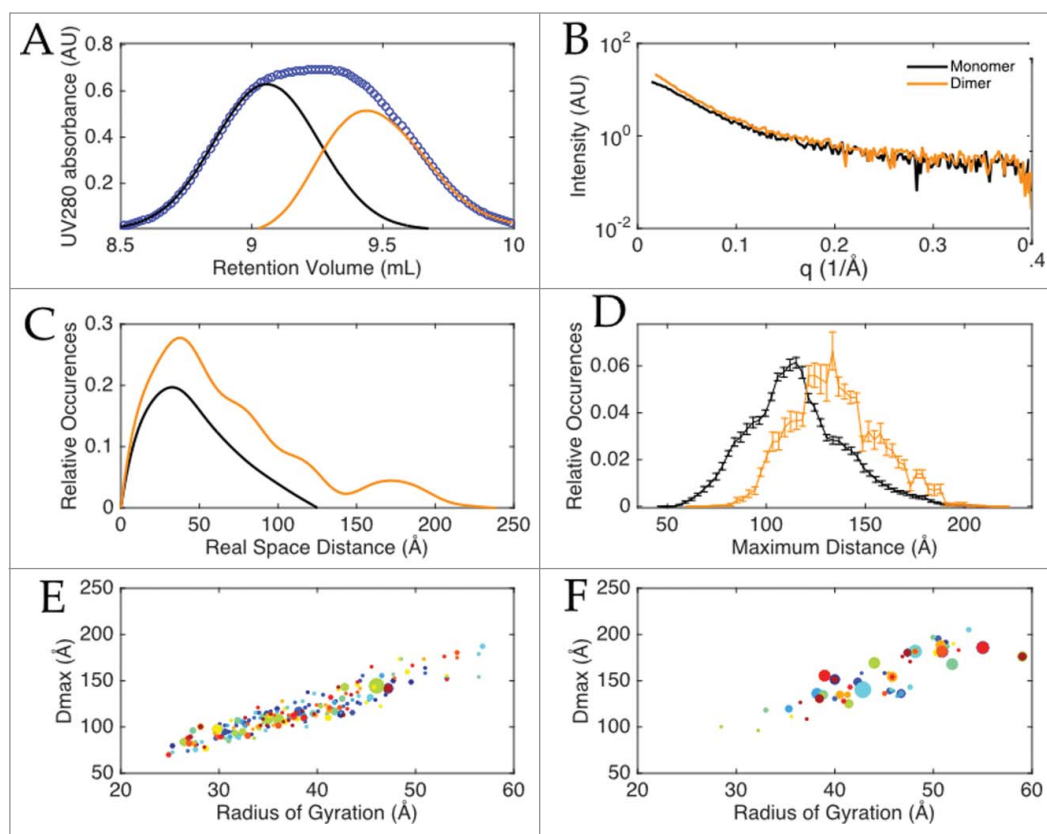
While the reported observation of Y39-Y39 αSN dimers has been made under ambient conditions, it does not exclude that the redox process, facilitatin the dimer formation, must have involved the presence of an original αSNY39•, i.e., a free radical. If such a free radical is formed prior to the SEC step, it could result in dimer-formation while passing over the column matrix. We have tested this hypothesis by electron paramagnetic resonance spectroscopy analysis, but if the free radical is present, prior to loading on the column, it is below detection limit (data not shown). This leads to the suggestion that the αSNY39• free radical is a short-lived species, and that the partial immobilization while passing over the column facilitates the formation of dimers.

In a recent study, Curtain and co-workers analyse analyze the structural distribution of αSN and familial mutants, from gel filtrated samples.[33] In that study, however, there is no notion of the presence of a bimodal elution profile from the size exclusion column. Although the authors do not allude to the possibility of a mixed pool of monomers and dimers, it is interesting to note that the authors describe a bimodal distribution of structures in the ensembles. The authors suggest that αSN adapts to two distinct monomer pools of compact and extended conformations, which is not in accordance with our current analysis, which reveals that monomeric αSN adapts to a near-random conformation. The results from Curtain et al. would be compatible with our results, if the extended pool represents un-detected dimers. It is not evident from the publication whether this option has been tested in the fitting procedures.

Here, in addition to unequivocally detecting the presence of dimeric structures under mild conditions (**Fig. 5**), we investigate the structural characteristics of the dimeric structures (**Fig. 7**). We show that the dimers increased affinity for the hydrophobic ANS probe (**Fig. 1**) correlates with the generation of a structural state, where a limited structural core is well defined, although not exhibiting secondary structural elements (see graphical abstract). We also show that the dimeric structural ensemble can be described from only a small number of structural conformations (**Fig. 7F**), which is in stark contrast to the much more widely distributed conformations of the monomeric structure (**Fig. 7E**). These dimeric structures, interestingly, are structurally distinct, and do not spatially overlap (see graphical abstract). Although still not adhering to a well-defined structure, such defined structures are likely to exhibit modified solution properties and, importantly, altered aggregation profiles in comparison with the much less defined monomeric structure. Indeed we see that the increased occurrence of the dimeric structure results in different aggregation kinetics.

Oxidation of methionines has been shown to inhibit fibrillation.[55] For o-o′-di-tyrosines, both faster kinetics[20] as well as unchanged aggregation rates, but decreased max fluorescence, have been reported.[56] Here, we initially observe highly similar kinetics, but the type3 preparation has a biphasic pattern. This could be due to 2 different aggregation pathways taking place with different rates. The fact that the second aggregation pathway is slower, as opposed to the previously reported faster kinetics,[20] can be explained by the relative lower amount of dimer compared to monomer. Krishnan and co-workercoworkers[20] worked with

fully oxidized samples whereas type3 samples are a mixture of monomer and dimers with the monomer constituting the majority of sample as judged from the SEC-chromatograms and bulk SAXS measurements. We did not observe any significant difference in maximum fluorescence, which is likely due to the lower concentration of the di-tyrosine compared to previous results.[57] Another explanation could also be that we only observe a specific di-tyrosine in contrast to the different di-tyrosines reported by Borsarelli and co-workers.[57] In spite of the altered kinetics of amyloid-like fibril formation for αSN type3, the fibril core appears unaltered, as investigated by fibre fiber diffraction.

It is natural to consider the potential role of di-tyrosines in PD, considering their occurrence under mild experimental conditions and their ability to affect the fibrillation rates. Oxidative stress has often been linked to neurodegenerative diseases.[2,26,58,59] Pennathur et al. reported the presence of o,o′-di-tyrosines in brains of PD animal models;[60] the level of reactive oxygen species were shown to be increased in SH-SY5Y cells overexpressing αSN[61], and Paxinou et al. showed that increased oxidative stress in the brain triggered αSN aggregation in HEK 293 cells.[62] It is hence not unreasonable to expect that di-tyrosine linked dimers can occur *in vivo* in the human brain in connection to PD. Oxidized αSN has indeed been detected *ex vivo* in brain slices from diseased patients suffering from dementia with LB[63] as well as in mouse models where reduction in microglia-derived nitric oxide and superoxide provided substantial neuroprotection[64]. It is thus relevant to further study the *in vivo* role of the covalent dimer presented in this paper, to investigate the potential role in the pathogenesis of PD and other synucleopathies.

Materials and Methods

Protein expression and purification

Recombinant αSN was expressed in *Escherichia coli* BL21 (DE 3) cell lines transfected with the plasmid vector p-ET11. The expression construct was a kind gift from Bioneer, Hørsholm, Denmark. Recombinant αSN was harvested from the periplasm by resuspending the cell pellets in an osmotic shock buffer (30 mM Tris, 40% sucrose, 2 mM EDTA, pH 7.2).[34] The lysate was subsequently boiled at 95 °C for a maximum of 15 minutes to precipitate impurities. The buffer was exchanged by dialysis with 20 mM Tris-HCl buffer pH 8.0 before being loaded onto a HiTrap Q FF ion-exchange column (GE Healthcare). Fractions containing αSN were identified with SDS-PAGE. The eluted fractions were divided into four 4 portions that were subsequently up-concentrated using centrifugal filter units (Millipore) to 3.5, 5.5 8.0 and 10 mg/ml respectively. These fractions were injected individually (2 mL per injection) onto a HiLoad Superdex 200 (GE Healthcare) to yield the protein batches αSN Type0-1-2-3 respectively. The collected fractions were dialyzed against MQ-water (Millipore) over-night. The protein was lyophilized and stored at −20°C. Fresh samples were prepared by re-dissolving αSN in 20 mM PBS buffer (150 mM NaCl, 20 mM NaPi, pH 7.4). The concentration was

determined by A_{280nm} ($\varepsilon = 5120$ $M^{-1}cm^{-1}$)[30] after filtration through 0.20 µm spin filters (Millipore).

Circular dichroism

Measurement on readily dissolved αSN was performed in the far-UV region on a Jasco J-715 spectropolarimeter equipped with a Jasco PCT 348 WI temperature controller. The temperature was kept constant at 25°C. Measurements were conducted in 0.1 mm quartz cuvettes in the region of 195–250 nm using 2.5 mg/ml αSN samples. Spectra were recorded sequentially with a 1 nm bandwidth and 0.1 nm data pitch. The scan speed was 50 nm/min and the total spectra were collected as an average of 8 accumulations.

Fluorescence measurements

Fluorescence spectra and excitation profiles measurements were carried out on a Jasco FP-8500 spectrofluorimeter equipped with a peltier thermostat (25°C). The measurements were performed in 1 cm quartz cuvettes at protein concentrations of 2.5 mg/ml.

Emission spectra of Anilino-1-naphthalene-sulfonate (Sigma Aldrich) (ANS) were recorded under excitation at 380 nm after thermal equilibration at 25°C. Scan-speed was 100 nm/min and integration time of 1 s, data pitch was 0.5 nm and emission and excitation bandwidth were 5 nm. The emission spectra were recorded once the fluorescence had stabilized after each added aliquot of ANS.

Freshly dissolved αSN was titrated with ANS. The ANS stock was prepared in PBS buffer ($\varepsilon = 5000$ $M^{-1}cm^{-1}$)[65]. The protein stocks (2.5 mg/ml) were titrated with aliquots of ANS varying [ANS]/[protein] molar ratio in the range 0–6. Dilutions on ANS never exceeded 5% of the starting volume.

Intrinsic fluorescence signal of protein samples was measured with excitation and emission bandwidths of 2.5 nm and 5 nm respectively. Scan-speed was 100 nm/min and integration time 1s. 3D fluorescence spectra were obtained in the emission range 270–400 nm scanning the excitation wavelength in the range 265–650 nm with 10 nm step.

Protein fibrillation

αSN was fibrillated in 96 well clear bottom plates (NUNC) on a Floustar Optima Platereader (BMG labtech). Fibrillation was performed in triplicates at 12 mg/ml with 20 uM Thioflavin T (ThT) (Sigma Aldrich) as fluorescent marker and a sample volume of 150 µL per well. The assays were conducted using same conditions used in Giehm et al.[66] including heating (37°C), shaking (orbital shaking, 300 rpm, 2 mm) in cycles of 280 sec followed by 80 sec pause. Each well contained a 3 mm glass bead to increase reproducibility.[35] ThT fluorescence was employed as an internal clock of the progress of protein amyloid fibrillation.[67,68] The emission was recorded at 480±5 nm after excitation at 450±5 nm.

Standard SAXS data collection and primary analysis

SAXS data from αSN samples were collected at the I911-SAXSbeamline at MAX-lab, Lund, Sweden, with the scattering intensity (I) as a function of the scattering vector ($q = 4\pi sin(\theta)/\lambda$).[69] The scattering was detected with a Pilatus 1 M detector in a momentum transfer range of 0.008–0.44 Å^{-1} with 120 sec of exposure. Measurements were performed at 8°C and the samples were oscillated during exposure to avoid radiation damage. The signal was scaled by the intensity of the transmitted beam. The bioXtas software RAW[70] was applied to transform the data from 2D to 1D by radial averaging. The scattering from an identical PBS buffer was subtracted to obtain the isolated protein scattering. The scattering of protein samples at 3, 7 and 12 mg/ml were measured to ensure that protein-protein interactions did not introduce artifacts at low scattering angles and to check for potential further concentration induced dimerization. The extrapolated forward scattering (I(0)) and radius of gyration (R_g) were determined using PRIMUS from the ATSAS suite[71] and as no protein-protein interaction was observed in the given concentration range, the scattering from the 12 mg/ml samples was used in the further analyses. The data were analyzed with EOM[71,72] to test if the data could be fitted to an ensemble of structures from a pool of structures resembling natively unfolded protein: The valid Guinier range was used to determine the q_{min} for the EOM analysis ($q*R_g \leq 1.3$) and data points above $q = 0.3$ Å^{-1} were excluded. A pool of 1000 structures resembling an intrinsically disordered protein with the primary structure of αSN was generated using the RANCH procedure within EOM. Equivalently we generated 3 different dimer pools with respective dimer contact points in either the C-terminal (including Y125, Y133 and Y136), the NAC-region (residues 61–95)[73] or at Y39. Using the genetic algorithm GAJOE, we tested fitting of the experimental scattering data to selected ensembles from individual pools of monomers and dimers as well as combined pools including both monomers and dimers. 1000 generations were completed for each pool with 100 repeats. The maximum ensemble size was restricted to 50 entities.

Mass spectrometry

Iodocetamide (IAM) ≥ 99%, dithiothreitol (DTT) ≥ 99.5%, 1,4 dicyanobenzene (98%) and trypsin were of proteomics grade from Sigma Aldrich. All other chemicals or reagents were at least of analytical grade. Tryptic digestion was performed on samples containing 600 pmol of αSN. The protein was denatured by incubation with denaturation buffer [50 mM ammonium bicarbonate, 6 M GndHCl, pH 8.0] (60°C, 30 min) followed by reduction with 13.7 mM DTT (60°C, 3 h) and alkylation with 23.3 mM IAM (RT, 30 min). Samples were then diluted with digestion buffer [50 mM ammonium bicarbonate, pH 8.0] containing 100 mM $CaCl_2$. Trypsin (5 µM) was added to obtain a final amount of 1/20 (trypsin/protein, w/w) in total 200 µL sample solutions. The samples were then incubated overnight at 37°C.

LC-MS was performed using a NanoAQUITY UPLC setup coupled to an ESI Synapt G2 Q-TOF mass spectrometer (Waters). Samples of tryptic digests were loaded onto the UPLC system and trapped and desalted on a C18 trap column (ACQUITY UPLC BEH C18 1.7 µm VanGuard column, Waters) for 3 min at 150 µL/min of mobile phase A (0.23% Formic Acid).

Peptides were subsequently eluted across a C18 analytical column (ACQUITY UPLC BEH C18 1.7 μm 1.0 × 100 mm column, Waters) and into the mass spectrometer using a gradient from 8% to 92% of mobile phase B (ACN, 0.23% Formic Acid) at a flow-rate of 40 μL/min.

MS was carried out in positive ion mode, with internal mass-calibration using a reference lock-spray signal of Glu-Fibrinopeptide (Sigma Aldrich). Peptide identification was performed by Data-Dependent Acquisition (DDA) Collision-Induced Dissociation (CID) MS/MS. Mass spectra were acquired over a m/z range of 50–2000. Electron Transfer Dissociation (ETD) MS/MS experiments were performed at optimized conditions (capillary voltage 2.8 kV, desolvation gas flow 800 L/h, cone gas flow 0 L/h, source temperature 90°C, desolvation gas temperature 300°C, sampling cone 20 V, extraction cone 2 V, T-wave Wave height 0.2 V and wave velocity 300 m/sec). ETD reagent (1,4-dicyanobenzene) was introduced into the glow discharge anion source using a flow of nitrogen makeup gas (20 mL/min) over the reagent crystals stored in a seal vial. The radical anions of the ETD reagent were generated via glow discharge using a current of 45 μA. ETD MS/MS data were acquired over 0.5 sec scans. Chromatograms and mass spectra were processed by MassLynx software (Waters, Miliford, USA). PLGS (ProteinLynx Global Server) ver. 3.0 (Waters, Miliford, USA) was used for peptide identification.

SEC-SAXS

Recording of SAXS data during size exclusion gel-filtration chromatography (SEC-SAXS) was carried out at the BioSAXS beamline BM29 at the European Synchrotron Radiation Facility (ESRF), Grenoble, France.[41] Samples with an expected high content of the altered αSN species (revealed as a chromatographic shoulder on the main peak) were prepared by dissolving protein from a type3 batch and up-concentrating it to 17 mg/ml. Using the automatic setup,[41] the sample was injected and SAXS data with exposures of 1 sec/frame was recorded continuously throughout the gel filtration. Standard PBS was used as the elution buffer. The recorded 2D images were radially averaged by the beamline software pipeline.[41] Data were reduced and analysed analyzed using Matlab 8.4 (The MathWorks IncInc.). Briefly, a data curve representing the buffer component was produced, by averaging several buffer data curves before the peak but after the void volume. The buffer component was then used for background subtraction from data collected while the chromatographic peak eluted. Data from the expected monomeric species were constructed as an average of the initial 9 data-frames, and it was validated by the Guinier approximation that all individual data frames (before averaging) had stable R_g values. If assuming that only the monomer was present throughout the elution profile, large systematic trends in the residual scattering curves revealed that one component was not enough to explain the data. A new decomposition was done using the monomer data and an altered species component. The altered species component was isolated in the following way: The elution profile of the second species was initially estimated by a Gaussian decomposition of the UV-trace. Based on this, a region expectedly corresponding to a pure second component was selected. Consistent scattering profiles confirmed the validity of the selected region. A linear combination of these two species throughout the elution profile left negligible residual scattering profiles, and it was concluded that the profile could be explained by two components. Molar mass approximation from the Guinier approximation was also employed. EOM analysis was performed on the Y39-Y39 dimer pool (as described above) and running the genetic algorithm 12 times using the same initial pool. The pair distance distribution function was obtained using GNOM from the ATSAS suite.[71]

Supplemental Material
Supplemental data for this article can be accessed on the publisher's website.

References

1. Eisenberg D, Jucker M. The amyloid state of proteins in human diseases. Cell 2012; 148:1188-203; PMID:22424229; http://dx.doi.org/10.1016/j.cell.2012.02.022

2. Hwang O. Role of oxidative stress in Parkinson's disease. Exp Neurobiol 2013; 22:11-7; PMID:23585717; http://dx.doi.org/10.5607/en.2013.22.1.11

3. Spillantini MG, Schmidt ML, Lee VM, Trojanowski JQ, Jakes R, Goedert M. Alpha-synuclein in Lewy bodies. Nature 1997; 388:839-40; PMID:9278044; http://dx.doi.org/10.1038/42166

4. Lashuel HA, Overk CR, Oueslati A, Masliah E. The many faces of alpha-synuclein: from structure and toxicity to therapeutic target. Nat Rev Neurosci 2013; 14:38-48; PMID:23254192; http://dx.doi.org/10.1038/nrn3406

5. Burre J, Vivona S, Diao J, Sharma M, Brunger AT, Sudhof TC. Properties of native brain alpha-synuclein. Nature 2013; 498:107-10; http://dx.doi.org/10.1038/nature12125

6. Fauvet B, Mbefo MK, Fares M-B, Desobry C, Michael S, Ardah MT, Tsika E, Coune P, Prudent M, Lion N, et al. α-synuclein in central nervous system and from erythrocytes, mammalian cells, and escherichia coli exists predominantly as disordered monomer. J Biol Chem 2012; 287:15345-64; PMID:22315227; http://dx.doi.org/10.1074/jbc.M111.318949

7. Burré J, Sharma M, Tsetsenis T, Buchman V, Etherton MR, Südhof TC. α-synuclein promotes SNARE-complex assembly in vivo and in vitro. Science 2010; 329:1663-7; http://dx.doi.org/10.1126/science.1195227

8. Lai Y, Kim S, Varkey J, Lou X, Song J-K, Diao J, Langen R, Shin Y-K. Nonaggregated α-synuclein influences SNARE-dependent vesicle docking via membrane binding. Biochemistry 2014; 53:3889-96; PMID:24884175; http://dx.doi.org/10.1021/bi5002536

9. Burré J, Sharma M, Südhof TC. α-Synuclein assembles into higher-order multimers upon membrane binding to promote SNARE complex formation. Proc of the Natl Acad of Sci 2014; 111:E4274-E83; http://dx.doi.org/10.1073/pnas.1416598111

10. Herva ME, Spillantini MG. Parkinson's disease as a member of Prion-like disorders. Virusr Research 2014; PMID:25456401

11. Winner B, Jappelli R, Maji SK, Desplats PA, Boyer L, Aigner S, Hetzer C, Loher T, Vilar M, Campioni S, et al. In vivo demonstration that α-synuclein oligomers are toxic. Proc of the Natl Acad of Sci 2011; 108:4194-9; http://dx.doi.org/10.1073/pnas.1100976108

12. Dimant H, Kalia SK, Kalia LV, Zhu LN, Kibuuka L, Ebrahimi-Fakhari D, McFarland NR, Fan Z, Hyman BT, McLean PJ. Direct detection of alpha synuclein oligomers in vivo. Acta Neuropathol Commun 2013; 1:6; PMID:24252244; http://dx.doi.org/10.1186/2051-5960-1-6

13. Conway KA, Lee S-J, Rochet J-C, Ding TT, Williamson RE, Lansbury PT. Acceleration of oligomerization, not fibrillization, is a shared property of both α-synuclein mutations linked to early-onset Parkinson's disease: implications for pathogenesis and therapy. Proc of the Natl Acad of Sci 2000; 97:571-6; http://dx.doi.org/10.1073/pnas.97.2.571

14. Klein C, Westenberger A. Genetics of Parkinson's disease. Cold Spring Harb Perspect Med 2012; 2; PMID:22315721; http://dx.doi.org/10.1101/cshperspect.a008888

15. Kasten M, Klein C. The many faces of alpha-synuclein mutations. Mov Disord 2013; 28:697-701; PMID:23674458; http://dx.doi.org/10.1002/mds.25499

16. Antony PMA, Diederich NJ, Krüger R, Balling R. The hallmarks of Parkinson's disease. FEBS J 2013; 280:5981-93; PMID:23663200; http://dx.doi.org/10.1111/febs.12335

17. Breydo L, Wu JW, Uversky VN. α-Synuclein misfolding and Parkinson's disease. Biochimica et Biophysica Acta (BBA) - Molecular Basis of Disease 2012; 1822:261-85; http://dx.doi.org/10.1016/j.bbadis.2011.10.002

18. Takahashi T, Yamashita H, Nakamura T, Nagano Y, Nakamura S. Tyrosine 125 of α-synuclein plays a critical role for dimerization following nitrative stress. Brain Res 2002; 938:73-80; PMID:12031537; http://dx.doi.org/10.1016/S0006-8993(02)02498-8

19. Souza JM, Giasson BI, Chen Q, Lee VM-Y, Ischiropoulos H. Dityrosine cross-linking promotes formation of stable α-synuclein polymers: implications of nitrative and oxidative stress in the pathogenesis of neurodegenerative synucleinopathies. J Biol Chem 2000; 275:18344-9; PMID:10747881; http://dx.doi.org/10.1074/jbc.M000206200

20. Krishnan S, Chi EY, Wood SJ, Kendrick BS, Li C, Garzon-Rodriguez W, Wypych J, Randolph TW, Narhi LO, Biere AL, et al. Oxidative dimer formation is the critical rate-limiting step for parkinson's disease α-synuclein fibrillogenesis†. Biochemistry 2002; 42:829-37; http://dx.doi.org/10.1021/bi026528t

21. Andrekopoulos C, Zhang H, Joseph J, Kalivendi S, Kalyanaraman B. Bicarbonate enhances alpha-synuclein oligomerization and nitration: intermediacy of carbonate radical anion and nitrogen dioxide radical. Biochem J 2004; 378:435-47; PMID:14640973; http://dx.doi.org/10.1042/BJ20031466

22. Devi L, Raghavendran V, Prabhu BM, Avadhani NG, Anandatheerthavarada HK. Mitochondrial import and accumulation of α-synuclein impair complex i in human dopaminergic neuronal cultures and parkinson disease brain. J Biol Chem 2008; 283:9089-100; PMID:18245082; http://dx.doi.org/10.1074/jbc.M710012200

23. Martin LJ, Pan Y, Price AC, Sterling W, Copeland NG, Jenkins NA, Price DL, Lee MK. Parkinson's disease alpha-synuclein transgenic mice develop neuronal mitochondrial degeneration and cell death. J Neurosci 2006; 26:41-50; PMID:16399671; http://dx.doi.org/10.1523/JNEUROSCI.4308-05.2006

24. Bosco DA, Fowler DM, Zhang Q, Nieva J, Powers ET, Wentworth P, Lerner RA, Kelly JW. Elevated levels of oxidized cholesterol metabolites in Lewy body disease brains accelerate [alpha]-synuclein fibrillization. Nat Chem Biol 2006; 2:249-53; PMID:16565714; http://dx.doi.org/10.1038/nchembio782

25. Caudle WM, Colebrooke RE, Emson PC, Miller GW. Altered vesicular dopamine storage in Parkinson's disease: a premature demise. Trends Neurosci 2008; 31:303-8; PMID:18471904; http://dx.doi.org/10.1016/j.tins.2008.02.010

26. Dias V, Junn E, Mouradian MM. The role of oxidative stress in Parkinson's disease. J Parkinsons Dis 2013; 3:461-91; PMID:24252804

27. Berndt N, Holzhütter H-G, Bulik S. Implications of enzyme deficiencies on mitochondrial energy metabolism and reactive oxygen species formation of neurons involved in rotenone-induced Parkinson's disease: a model-based analysis. FEBS J 2013; 280:5080-93; PMID:23937586; http://dx.doi.org/10.1111/febs.12480

28. Dunker AK, Lawson JD, Brown CJ, Williams RM, Romero P, Oh JS, Oldfield CJ, Campen AM, Ratliff CM, Hipps KW. Intrinsically disordered protein. J of Mol Graph and Model 2001; 19:26-59; PMID:11381529; http://dx.doi.org/10.1016/S1093-3263(00)00138-8

29. Weinreb PH, Zhen W, Poon AW, Conway KA, Lansbury PT. NACP, a protein implicated in Alzheimer's disease and learning, is natively unfolded. Biochemistry 1996; 35:13709-15; PMID:8901511; http://dx.doi.org/10.1021/bi961799n

30. Eliezer D, Kutluay E, Bussell Jr R, Browne G. Conformational properties of α-synuclein in its free and lipid-associated states. J Mol Biol 2001; 307:1061-73; PMID:11286556; http://dx.doi.org/10.1006/jmbi.2001.4538

31. Waudby CA, Camilloni C, Fitzpatrick AWP, Cabrita LD, Dobson CM, Vendruscolo M, Christodoulou J. In-Cell NMR Characterization of the Secondary structure populations of a disordered conformation of α-synuclein within E. coli cells. PLoS One 2013; 8: e72286; PMID:23991082; http://dx.doi.org/10.1371/journal.pone.0072286

32. Rao JN, Jao CC, Hegde BG, Langen R, Ulmer TS. A combinatorial NMR and EPR approach for evaluating the structural ensemble of partially folded proteins. J of the Am Chem Soc 2010; 132:8657-68; PMID:20524659; http://dx.doi.org/10.1021/ja100646t

33. Curtain CC, Kirby NM, Mertens HD, Barnham KJ, Knott RB, Masters CL, Cappai R, Rekas A, Kenche VB, Ryan T. Alpha-synuclein oligomers and fibrils originate in two distinct conformer pools: a small angle X-ray scattering and ensemble optimisation modelling study. Mol Biosyst 2015; 11:190-6; PMID:25352253; http://dx.doi.org/10.1039/C4MB00356J

34. Huang C, Ren G, Zhou H, Wang CC. A new method for purification of recombinant human alpha-synuclein in Escherichia coli. Protein Expr Purif 2005; 42:173-7; PMID:15939304; http://dx.doi.org/10.1016/j.pep.2005.02.014

35. Giehm L, Otzen DE. Strategies to increase the reproducibility of protein fibrillization in plate reader assays. Anal Biochem 2010; 400:270-81; PMID:20149780; http://dx.doi.org/10.1016/j.ab.2010.02.001

36. Coelho-Cerqueira E, Carmo-Goncalves P, Pinheiro AS, Cortines J, Follmer C. alpha-Synuclein as an intrinsically disordered monomer-fact or artefact? FEBS J 2013; 280:4915-27; PMID:23927048; http://dx.doi.org/10.1111/febs.12471

37. Giehm L, Svergun DI, Otzen DE, Vestergaard B. Low-resolution structure of a vesicle disrupting α-synuclein oligomer that accumulates during fibrillation. Proc of the Natl Acad of Sci 2011; 108:3246-51; http://dx.doi.org/10.1073/pnas.1013225108

38. van Maarschalkerweerd A, Vetri V, Langkilde AE, Fodera V, Vestergaard B. Protein/lipid coaggregates are formed during alpha-synuclein-induced disruption of lipid bilayers. Biomacromolecules 2014; 15:3643-54; PMID:25210839; http://dx.doi.org/10.1021/bm500937p

39. Hawe A, Sutter M, Jiskoot W. Extrinsic fluorescent dyes as tools for protein characterization. Pharm Res 2008; 25:1487-99; PMID:18172579; http://dx.doi.org/10.1007/s11095-007-9516-9

40. Bolognesi B, Kumita JR, Barros TP, Esbjorner EK, Luheshi LM, Crowther DC, Wilson MR, Dobson CM, Favrin G, Yerbury JJ. ANS binding reveals common features of cytotoxic amyloid species. ACS Chem Biol 2010; 5:735-40; PMID:20550130; http://dx.doi.org/10.1021/cb1001203

41. Pernot P, Round A, Barrett R, De Maria Antolinos A, Gobbo A, Gordon E, Huet J, Kieffer J, Lentini M, Mattenet M. Upgraded ESRF BM29 beamline for SAXS on macromolecules in solution. J of Synchrotron Radiat 2013; 20:0-; http://dx.doi.org/10.1107/S0909049513010431

42. Vestergaard B, Groenning M, Roessle M, Kastrup JS, Van De Weert M, Flink JM, Frokjaer S, Gajhede M, Svergun DI. A helical structural nucleus is the primary elongating unit of insulin amyloid fibrils. PLoS Biology 2007; 5:e134; PMID:17472440; http://dx.doi.org/10.1371/journal.pbio.0050134

43. Frimpong AK, Abzalimov RR, Uversky VN, Kaltashov IA. Characterization of intrinsically disordered proteins with electrospray ionization mass spectrometry: conformational heterogeneity of α−synuclein. Proteins 2010; 78:714-22

44. Li C, Feany MB. a-Synuclein phosphorylation controls neurotoxicity and inclusion formation in a Drosophila model of Parkinson disease. Nat Neurosci 2005; 8:657-63; PMID:15834418; http://dx.doi.org/10.1038/nn1443

45. Slow EJ, Graham RK, Osmand AP, Devon RS, Lu G, Deng Y, Pearson J, Vaid K, Bissada N, Wetzel R, et al. Absence of behavioral abnormalities and neurodegeneration in vivo despite widespread neuronal huntingtin inclusions. Proc Natl Acad Sci U S A 2005; 102:11402-7; PMID:16076956; http://dx.doi.org/10.1073/pnas.0503634102

46. Sacino A, Brooks M, Thomas M, McKinney A, McGarvey N, Rutherford N, Ceballos-Diaz C, Robertson J, Golde T, Giasson B. Amyloidogenic α-synuclein seeds do not invariably induce rapid, widespread pathology in mice. Acta Neuropathol 2014; 127:645-65; PMID:24659240; http://dx.doi.org/10.1007/s00401-014-1268-0

47. Wang G, van der Walt JM, Mayhew G, Li Y-J, Züchner S, Scott WK, Martin ER, Vance JM. Variation in the miRNA-433 binding site of FGF20 confers risk for Parkinson disease by overexpression of α-synuclein. The Am J of Hum Genet 2008; 82:283-9; PMID:18252210; http://dx.doi.org/10.1016/j.ajhg.2007.09.021

48. Singleton AB, Farrer M, Johnson J, Singleton A, Hague S, Kachergus J, Hulihan M, Peuralinna T, Dutra A, Nussbaum R, et al. α-synuclein locus triplication causes Parkinson's disease. Science 2003; 302:841; PMID:14593171; http://dx.doi.org/10.1126/science.1090278

49. Horvath I, Weise CF, Andersson EK, Chorell E, Sellstedt M, Bengtsson C, Olofsson A, Hultgren SJ, Chapman MR, Wolf-Watz M. Mechanisms of protein oligomerization: in-hibitor of functional amyloids templates a-synuclein fibrilla-tion. J of the Am Chem Soc 2012; 134(7):3439-44; PMID:22260746; http://dx.doi.org/10.1021/ja209829m

50. Norris EH, Giasson BI, Ischiropoulos H, Lee VM-Y. Effects of oxidative and nitrative challenges on α-synuclein fibrillogenesis involve distinct mechanisms of protein modifications. J Biol Chem 2003; 278:27230-40; PMID:12857790; http://dx.doi.org/10.1074/jbc.M212436200

51. Dusa A, Kaylor J, Edridge S, Bodner N, Hong DP, Fink AL. Characterization of oligomers during alpha-synuclein aggregation using intrinsic tryptophan fluorescence. Biochemistry 2006; 45:2752-60; PMID:16489768; http://dx.doi.org/10.1021/bi051426z

52. Harms G, Pauls S, Hedstrom J, Johnson C. Fluorescence and rotational dynamics of dityrosine. J Fluoresc 1997; 7:283-92; http://dx.doi.org/10.1023/A:1022525909128

53. Aeschbach R, Amado∫ R, Neukom H. Formation of dityrosine cross-links in proteins by oxidation of tyrosine residues. Biochim Biophys 1976; 439:292-301; http://dx.doi.org/10.1016/0005-2795(76)90064-7

54. Malencik DA, Sprouse JF, Swanson CA, Anderson SR. Dityrosine: preparation, isolation, and analysis. Anal Biochem 1996; 242:202-13; PMID:8937563; http://dx.doi.org/10.1006/abio.1996.0454

55. Uversky VN, Yamin G, Souillac PO, Goers J, Glaser CB, Fink AL. Methionine oxidation inhibits fibrillation of human alpha-synuclein in vitro. FEBS Lett 2002; 517:239-44; PMID:12062445; http://dx.doi.org/10.1016/S0014-5793(02)02638-8

56. Borsarelli CD, Falomir-Lockhart LJ, Ostatna V, Fauerbach JA, Hsiao HH, Urlaub H, Palecek E, Jares-Erijman EA, Jovin TM. Biophysical properties and cellular toxicity of covalent crosslinked oligomers of alpha-synuclein formed by photoinduced side-chain tyrosyl radicals. Free Radical Biol Med 2012; 53:1004-15; PMID:22771470; http://dx.doi.org/10.1016/j.freeradbiomed.2012.06.035

57. Borsarelli CD, Falomir-Lockhart LJ, Ostatná V, Fauerbach JA, Hsiao H-H, Urlaub H, Paleček E, Jares-Erijman EA, Jovin TM. Biophysical properties and cellular toxicity of covalent crosslinked oligomers of α-synuclein formed by photoinduced side-chain tyrosyl radicals. Free Radical Biol and Med 2012; 53:1004-15; PMID:22771470; http://dx.doi.org/10.1016/j.freeradbiomed.2012.06.035

58. Andersen JK. Oxidative stress in neurodegeneration: cause or consequence? Nat Rev Neurosci 2004; 5:S18-S25; http://dx.doi.org/10.1038/nrn1434

59. Ischiropoulos H. Oxidative modifications of α-synuclein. Ann N Y Acad Sci 2003; 991:93-100; PMID:12846977; http://dx.doi.org/10.1111/j.1749-6632.2003.tb07466.x

60. Pennathur S, Jackson-Lewis V, Przedborski S, Heinecke JW. Mass spectrometric quantification of 3-nitrotyrosine, ortho-tyrosine, and o,o′-dityrosine in brain tissue of 1-methyl-4-phenyl-1,2,3,6-tetrahydropyridine-treated mice, a model of oxidative stress in Parkinson's disease. J Biol Chem 1999; 274:34621-8; PMID:10574926; http://dx.doi.org/10.1074/jbc.274.49.34621

61. Junn E, Mouradian MM. Human α-Synuclein overexpression increases intracellular reactive oxygen species levels and susceptibility to dopamine. Neurosci Lett 2002; 320:146-50; PMID:11852183; http://dx.doi.org/10.1016/S0304-3940(02)00016-2

62. Paxinou E, Chen Q, Weisse M, Giasson BI, Norris EH, Rueter SM, Trojanowski JQ, Lee VM, Ischiropoulos H. Induction of alpha-synuclein aggregation by intracellular nitrative insult. J Neurosci 2001; 21:8053-61; PMID:11588178

63. Duda JE, Giasson BI, Mabon ME, Lee VMY, Trojanowski JQ. Novel antibodies to synuclein show abundant striatal pathology in Lewy body diseases. Ann Neurol 2002; 52:205-10; PMID:12210791; http://dx.doi.org/10.1002/ana.10279

64. Gao H-M, Kotzbauer PT, Uryu K, Leight S, Trojanowski JQ, Lee VM-Y. Neuroinflammation and oxidation/nitration of α-synuclein linked to dopaminergic neurodegeneration. J Neurosci 2008; 28:7687-98; PMID:18650345; http://dx.doi.org/10.1523/JNEUROSCI.0143-07.2008

65. Stryer L. The interaction of a naphthalene dye with apomyoglobin and apohemoglobin. A fluorescent probe of non-polar binding sites. J Mol Biol 1965; 13:482-95; PMID:5867031; http://dx.doi.org/10.1016/S0022-2836(65)80111-5

66. Giehm L, Lorenzen N, Otzen DE. Assays for alpha-synuclein aggregation. Methods 2011; 53:295-305; PMID:21163351; http://dx.doi.org/10.1016/j.ymeth.2010.12.008

67. Groenning M. Binding mode of Thioflavin T and other molecular probes in the context of amyloid fibrils—current status. J Chem Biol 2010; 3:1-18; PMID:19693614; http://dx.doi.org/10.1007/s12154-009-0027-5

68. Langkilde AE, Vestergaard B. Structural characterization of prefibrillar intermediates and amyloid fibrils by small-angle X-ray scattering. Methods Mol Biol 2012; 849:137-55; PMID:22528088; http://dx.doi.org/10.1007/978-1-61779-551-0_10

69. Blanchet CE, Svergun DI. Small-angle X-ray scattering on biological macromolecules and nanocomposites in solution. Annu Rev Phys Chem 2013; 64:37-54; PMID:23216378; http://dx.doi.org/10.1146/annurev-physchem-040412-110132

70. Nielsen SS, Toft KN, Snakenborg D, Jeppesen MG, Jacobsen JK, Vestergaard B, Kutter JP, Arleth L. BioXTAS RAW, a software program for high-throughput automated small-angle X-ray scattering data reduction and preliminary analysis. J Appl Crystallogr 2009; 42:959-64; http://dx.doi.org/10.1107/S0021889809023863

71. Petoukhov MV, Franke D, Shkumatov AV, Tria G, Kikhney AG, Gajda M, Gorba C, Mertens HD, Konarev PV, Svergun DI. New developments in the ATSAS program package for small-angle scattering data analysis. J Appl Crystallogr 2012; 45:342-50; PMID:25484842; http://dx.doi.org/10.1107/S0021889812007662

72. Bernado P, Svergun DI. Structural analysis of intrinsically disordered proteins by small-angle X-ray scattering. Mol Biosyst 2012; 8:151-67; PMID:21947276; http://dx.doi.org/10.1039/C1MB05275F

73. Stefanis L. alpha-synuclein in Parkinson's disease. Cold Spring Harb Perspect Med 2012; 2:a009399; PMID:22355802; http://dx.doi.org/10.1101/cshperspect.a009399